CHEMICAL DYNAMICS

Stereodynamical control of the H + HD → H_2 + D reaction through HD reagent alignment

Yufeng Wang[1]†, Jiayu Huang[1]†, Wei Wang[1,2], Tianyu Du[1,2], Yurun Xie[1,3], Yuxin Ma[1,2], Chunlei Xiao[1,4]*, Zhaojun Zhang[1]*, Dong H. Zhang[1,3,4]*, Xueming Yang[1,3,4]*

Prealigning nonpolar reacting molecules leads to large stereodynamical effects because of their weak steering interaction en route to the reaction barrier. However, experimental limitations in preparing aligned molecules efficiently have hindered the investigation of steric effects in bimolecular reactions involving hydrogen. Here, we report a high-resolution crossed-beam study of the reaction H + HD(v = 1, j = 2) → H_2(v', j') + D at collision energies of 0.50, 1.20, and 2.07 electron volts in which the vibrationally excited hydrogen deuteride (HD) molecules were prepared in two collision configurations, with their bond preferentially aligned parallel and perpendicular to the relative velocity of collision partners. Notable stereodynamical effects in differential cross sections were observed. Quantum dynamics calculations revealed that strong constructive interference in the perpendicular configuration plays an important role in the stereodynamical effects observed.

The fundamental goal for chemical reaction dynamics is to provide a detailed and quantitative understanding of the chemical reaction process and to provide new tools to control the outcome of a chemical event beyond the traditional ways, such as adding suitable catalysts and changing the temperature or pressure of a reaction mixture. One efficient way to control chemical reactions is to deposit some energy in the reaction coordinate of the reactant to make a desired molecular bond more easily cleaved (*1*–*4*). Numerous dynamical studies have been carried out to realize such an idea through vibrational excitation of reagent molecules, leading to the discovery and deep understanding of bond-selective or mode-specific chemistry (*5*–*7*). In addition to vibrational control, it is well established that the mutual orientation of the colliding partners also has a big effect on the chemical reaction outcome. Hence, by controlling colliding molecular orientation, it is possible to either promote or hinder the yield of products into specific final states or scattering angles (*8*–*10*).

For many years, steric control has been performed for inelastic and reactive systems mainly involving polar molecules (*11*–*13*). Many methods have been developed for aligning or orienting molecules in scattering experiments, including optical pumping (*14*), hexapole state selection (*15*), and brute force orientation (*16*). An elegant theoretical framework for the characterization of steric effects has been developed by Aldegunde *et al*. and Jambrina *et al*. (*17*, *18*). Recently, Heid *et al*. investigated end-on and side-on collisions of Ar with oriented NO and demonstrated that the collision outcome could be controlled by varying the bond axis orientation (*19*). Wang *et al*. and Pan *et al*. carried out a series of experiments to probe the steric effect on the differential cross sections (DCSs) in the Cl + CHD_3 reaction (*20*–*22*). A strong steric effect was observed, which suggests that reorientation effects of CHD_3 en route to the reaction barrier are not strong in this system owing to the essentially nonpolar nature of CHD_3 (*23*).

Clearly, aligning nonpolar reacting molecules can have large steric effects because of their weak steering interaction en route to the reaction barrier. H_2 is undoubtedly the best candidate for the purpose because it is both the most widely studied molecule in dynamical experiments and the most tractable theoretically (*24*–*27*). However, until recently, it has been difficult to prepare sufficient concentrations of H_2 in specific quantum states for scattering experiments (*28*, *29*). The development of the Stark-induced adiabatic Raman passage (SARP) technique not only opened the door to exciting a large concentration of H_2 and its isotopologues in specific quantum states to study collision dynamics for vibrationally excited H_2 molecules, but it also made it possible to align these molecules for steric dynamics experiments (*30*–*32*). Perreault *et al*. observed a strong stereodynamic preference of angular distributions in the inelastic scattering between aligned HD and D_2 molecules at temperatures down to 1 K (*33*), which indicates that the weak steering interaction can suppress the reorientation effects and expose more pronounced steric effects (*34*). They also created a quantum mechanical double slit by preparing the rovibrationally excited D_2 molecule in a biaxial state with coherently coupled bond axis orientations and demonstrated that they act as the two slits of a double-slit interferometer manifesting interference as a strong modulation in the measured angular distribution when inelastic scattering with a He atom (*35*, *36*). It would be highly desirable to see whether such striking steric effects can be observed in the simplest chemical reactions involving H_2 molecules and can be understood at the most fundamental level.

Experimental demonstration of stereodynamical control

We carried out a fully quantum state–resolved, crossed–molecular beam study for the H + HD → H_2 + D reaction, with HD molecules prepared in two preferentially aligned states using the stimulated Raman pumping (SRP) scheme. We found that the DCS of the reaction changed drastically with the direction of the HD bond axis, which indicated that we could effectively control the DCS of chemical reactions.

The experiment was conducted on a modified crossed-beam apparatus based on the Rydberg D atom time-of-flight (TOF) detection technique (*37*), as described in the supplementary materials. The HD beam was generated by supersonic expansion through a pulsed valve cooled by liquid nitrogen. The H beam was produced by ultraviolet laser photolysis of HI molecules in a pure HI beam at the nozzle tip of another pulsed valve. The HD beam and the H beam were collimated by skimmers and then entered the scattering chamber, where they collided at a crossing angle of 90°. The velocity of the HD beam was 1250 m/s. The speeds of H beam were 11,230, 17,470, and 22,949 m/s, corresponding to collision energies of 0.50, 1.20, and 2.07 eV, respectively. The HD molecules were excited from (v = 0, j = 0) to (v = 1, j = 2) (where v is the vibrational quantum number and j is the rotational quantum number) by SRP through the S(0) transition at the center of the scattering region of the two molecular beams. A single–longitudinal mode, optical parametric oscillator-amplifier produced the high-energy Stokes laser, which was the key for the high SRP excitation efficiency (*38*). After the reaction, the D atoms produced from the reaction were excited to a high-lying Rydberg state at the crossing region, then flew ~318 mm before reaching the MCP detector, where they were field-ionized by an electric field applied between the MCP and a metal mesh. The

[1]State Key Laboratory of Molecular Reaction Dynamics, Dalian Institute of Chemical Physics, Chinese Academy of Sciences, Dalian, Liaoning 116023, China. [2]School of Chemical Sciences, University of Chinese Academy of Sciences, Beijing 100049, China. [3]Department of Chemistry and Shenzhen Key Laboratory of Energy Chemistry, Southern University of Science and Technology, Shenzhen 518055, China. [4]Hefei National Laboratory, Hefei 230088, China.
*Corresponding author. Email: chunleixiao@dicp.ac.cn (C.X.); zhangzhj@dicp.ac.cn (Z.Z.); zhangdh@dicp.ac.cn (D.H.Z.); xmyang@dicp.ac.cn (X.Y.)
†These authors contributed equally to this work.

ion signals were then amplified, discriminated, and recorded in the form of a TOF spectrum.

Figure 1 shows the schematic of the preparation of vibrationally excited HD in two different collision geometries, similar to the scheme used in (*33*). Linearly polarized pump and Stokes lasers with parallel directions of polarization were used, so the HD molecules were excited to the (v = 1, j = 2, m = 0) state with quantization axis along the laser polarization direction. Because the HD bond axis in the (v = 1, j = 2, m = 0) state was preferentially aligned parallel to the laser polarization direction, we were able to control the direction of the HD bond axis in scattering by changing the direction of the laser polarization. By setting the polarization direction of the pump and Stokes lasers parallel or perpendicular to the relative velocity of colliding partners, the bond axis of HD was preferentially aligned in parallel or perpendicular to the relative velocity. We named these two collision configurations parallel and perpendicular, respectively.

Figure 2, A to C, presents TOF spectra of the H + HD(v = 1, j = 2) → H_2 + D reaction in the sideways direction with HD(v = 1, j = 2) prepared in parallel and perpendicular configurations at collision energies of 0.50, 1.20, and 2.07 eV, respectively, measured on the scattering plane. Many sharp peaks were observed in the TOF spectra. Based on the conservation of momentum and energy, they could be assigned to various rovibrational states of H_2 products. It was obvious that TOF spectra obtained with parallel and perpendicular configurations were quite different.

By measuring TOF spectra at different scattering angles on the scattering plane, DCSs of the reaction on the plane were obtained. It should be noted that in the perpendicular configuration, the alignment of the HD molecular bond on the x axis breaks the scattering symmetry about the z axis. As a result, the measured DCS on the scattering plane differs from the conventional DCS, whose integration over the scattering angle θ gives the integral cross section. Figure 3, A and C, shows DCSs of H + HD(v = 1, j = 2) → H_2 + D obtained at the collision energy of 0.50 eV for parallel and perpendicular configurations, respectively. Even casual inspection reveals that the DCSs for these two configurations were different. For the parallel configuration, the H_2 products were predominantly backward scattered, with some small peaks for the products with low translational energy in the sideways direction. For the perpendicular configuration, the DCS showed pronounced sideways scattered peaks, in particular for the products with low translational energy. Evident differences between the two DCSs indicated the existence of strong stereodynamical effects in this reaction.

The difference in the DCSs for these two configurations at the collision energy of 1.20 eV was even more obvious. For the parallel configuration, the H_2 products remained predominantly backward scattered, whereas the sideway peaks became higher and some forward components showed up (Fig. 3E). In strong contrast, the angular distribution for the perpendicular configuration was dominated by sideways peaks (Fig. 3G) with backward-scattered amplitude suppressed substantially, underscoring strong stereodynamical effects in the reaction.

With a further increase of collision energy to 2.07 eV, the angular distributions for both the parallel and perpendicular configurations looked quite similar—dominated by sideways peaks with more or less the same scattering angles and the same translational energies (Fig. 3, I and K). However, the relative intensities for large-angle scattering and for forward scattering were much stronger for the parallel configuration.

Figure 3 also shows the change of relative reactivity for these two configurations. At low collision energies, the parallel configuration that leads to end-on collisions is predominant because of a narrow cone of acceptance and small impact parameters. As the collision energy increases, the side-on configurations become increasingly prevalent and sideways or forward scattering takes over with the broadening of the acceptance cone and the increasing of the impact parameters.

Quantum dynamical simulation of stereodynamical effect

To understand the strong stereodynamical effects in the reaction, we carried out nonadiabatic time-dependent wave packet calculations on the diabatic potential energy surface we constructed for this reaction (*39*). Details of the theoretical calculation can be found in

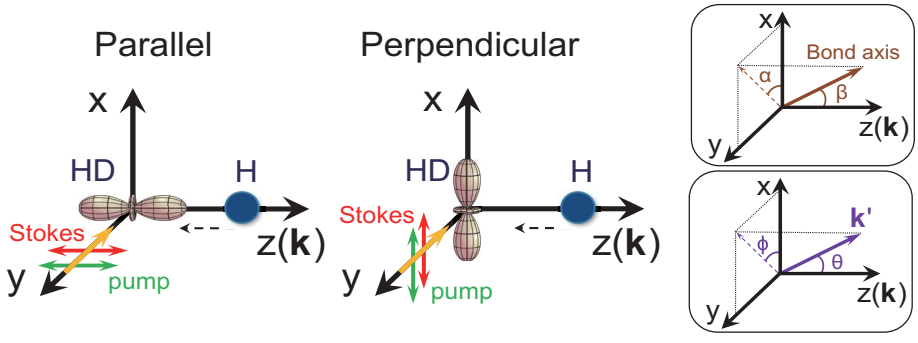

Fig. 1. The schematic of two collision geometries prepared by SRP. The scattering frame is defined so that the z axis is parallel to the reactant relative velocity, and xz is the detection plane (or scattering plane). The alignment of the molecular bond axis was controlled using the polarized pump and Stokes laser pulses, as indicated by the green and red double arrows, respectively. The preferential direction of the HD molecular bond axis in the scattering frame is specified by the polar and azimuthal angle (β, α). In theory, the direction of k′ is described by the polar and azimuthal angle (θ, ϕ). In the present experiment, ϕ = 0.

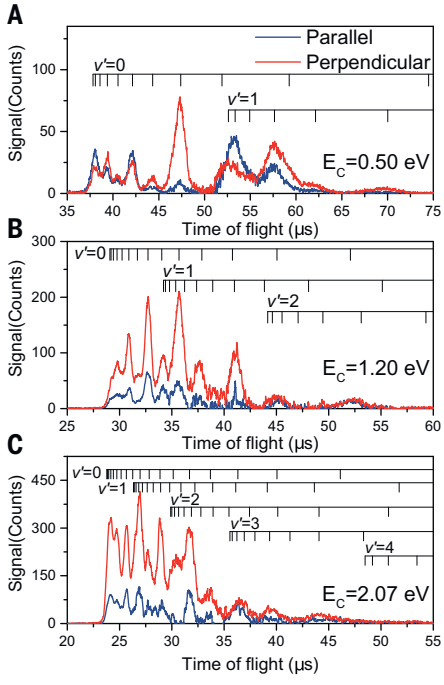

Fig. 2. TOF spectra of the D atom product from the H + HD(v = 1, j = 2) → H_2(v', j') + D reaction. (**A** to **C**) They were obtained at three collision energies: 0.50 eV (A), 1.20 eV (B), and 2.07 eV (C) in parallel (blue solid line) and perpendicular (red solid line) configurations in the sideways direction, at laboratory angles of 25° (A), 28° (B), and 29° (C), respectively. The sharp peaks can be assigned to various rovibrational states of the H_2 product, as indicated in the figure.

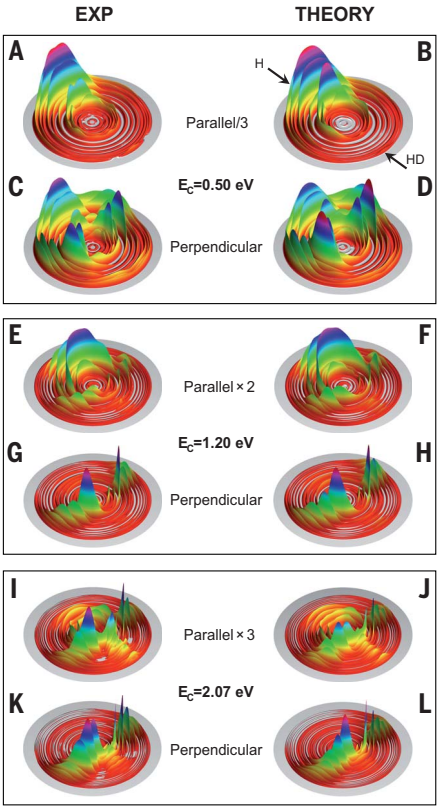

Fig. 3. Three-dimensional scattering H_2 product contour plots on the scattering plane. (**A** to **L**) Product contour plots are shown in the center-of-mass frame for experimental measurements (left column) and quantum dynamics calculations (right column) at collision energies of 0.50 eV [(A) to (D)], 1.20 eV [(E) to (H)], and 2.07 eV [(I) to (L)], with parallel [(A), (B), (E), (F), (I), and (J)] and perpendicular [(C), (D), (G), (H), (K), and (L)] configurations, respectively.

the supplementary materials. For the parallel configuration, the state of HD prepared by SRP is $|v=1, j=2, m=0\rangle$, and for the perpendicular configuration, the state of HD prepared is

$$|v=1, j=2, m_x=0\rangle = \sqrt{\frac{3}{8}}|v=1, j=2, m=+2\rangle - \frac{1}{2}|v=1, j=2, m=0\rangle + \sqrt{\frac{3}{8}}|v=1, j=2, m=-2\rangle \quad (1)$$

where m denotes the projection of angular momentum along the quantization axis z at the direction of relative velocity, and m_x denotes the component along the x axis. The DCS for the parallel configuration for an outgoing channel with specific quantum state $(v'j'm')$ has a cylindrical symmetry with respect to the z axis and can be evaluated easily as

$$\frac{d\sigma(v=1, j=2, m_z=0 \rightarrow v'j'm')}{d\Omega} = |f(v=1, j=2, m=0 \rightarrow v'j'm')|^2 \equiv |f_0|^2 \quad (2)$$

where $f(v=1, j=2, m=0 \rightarrow v'j'm')$ represents the state-to-state scattering amplitude within a solid angle dΩ along the direction (θ, ϕ) defined with respect to the quantization z axis, which is abbreviated as f_0 with the under script 0 denoting m = 0 and other index omitted. For the perpendicular configuration, the DCS results from the interference of the scattering amplitudes associated with the three input channels as follows

$$\frac{d\sigma(v=1, j=2, m_x=0 \rightarrow v'j'm')}{d\Omega} = \left|\sqrt{\frac{3}{8}}f(m=+2) - \frac{1}{2}f(m=0) + \sqrt{\frac{3}{8}}f(m=-2)\right|^2 = \frac{3}{8}|f_{+2}|^2 + \frac{1}{4}|f_0|^2 + \frac{3}{8}|f_{-2}|^2 + Re\left[\frac{3}{4}f_{+2}f_{-2}^* - \sqrt{\frac{3}{8}}f_{+2}f_0^* - \sqrt{\frac{3}{8}}f_{-2}f_0^*\right] \quad (3)$$

In Fig. 3, the theoretical DCSs at each collision energy and for the internuclear axis preparations are also shown. The excellent agreement between experiment and theory demonstrates the high accuracy of the quantum calculations.

Influence of quantum interference on stereodynamical effect

Given that the quantum dynamical simulation was capable of accurately reproducing the observed DCSs, we were confident of using theory to determine the physical origin of the strong stereodynamical effects. At the collision energy of 0.50 eV, the DCS for the parallel configuration was determined by single input channel with m = 0 and manifested a predominated backward feature, as shown in Fig. 4A, as a result of head-on collision dynamics. By contrast, the DCSs for m = ±2, which are the main input channels for the perpendicular configuration, peak at θ = 100°, indicative of peripheral dynamics with large impact-parameter collisions as can been seen from the opacity functions shown in fig. S12 and the dependence of DCS on the total angular momentum shown in figs. S13 to S15. The direct combination of the m = 0 and m = ±2 DCSs with ¼ and ¾ weights without the interference term shown in Eq. 3 gave rise to an essentially straight line with a small bump at θ = 90°. However, the actual DCS for perpendicular configuration showed an evident peak around θ = 90°, with a height considerably higher than the direct combination result, apparently as a result of the constructive interference between the m = 0 and m = ±2 channels. Therefore, the pronounced sideways peaks for the perpendicular configuration shown in Fig. 3C came from the constructive interference between the m = 0 and m = ±2 channels. It is worthwhile to point out that the interference term at the forward and backward directions is zero, as explained in the supplementary materials.

Figure 4B shows the angular distribution at the collision energy of 1.2 eV. Although the DCS for the parallel configuration was still backward dominated, it extended all the way up to the forward direction with a substantial amplitude. The DCS for m = ±2 channels

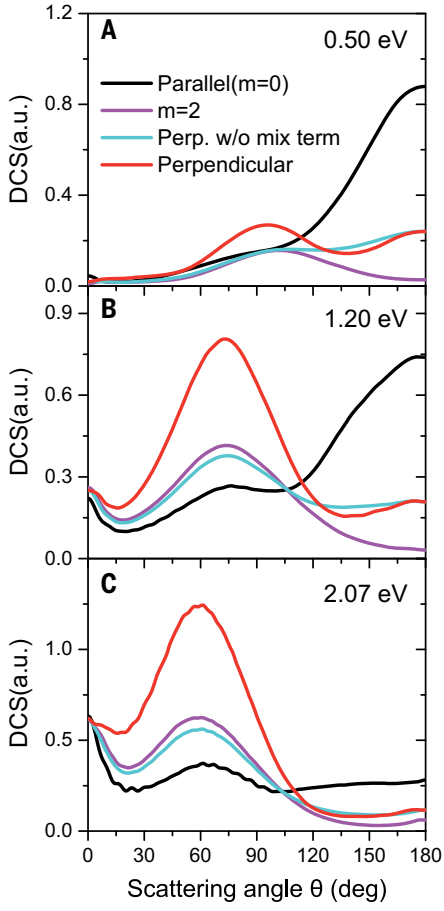

Fig. 4. Calculated DCSs on the scattering plane. (**A** to **C**) All final states of the H_2 product from the H + HD(v = 1, j = 2) → H_2 + D reaction are included at collision energies of 0.50 eV (A), 1.20 eV (B), and 2.07 eV (C), respectively. The results of m = −2 are equal to that of m = 2, so only m = 2 is shown. a.u., arbitrary units.

resembled that at the collision energy of 0.5 eV as a broad peak, but the peak position moved forward to θ = 70°. The direct combination of the m = 0 and m = ±2 DCSs without the interference terms resulted in a rather uniform distribution with a small but broad peak at θ = 70°. In strong contrast, the actual DCS had a pronounced peak also at θ = 70° with the amplitude doubled as compared with that without the interference terms because of the constructive interference between the m = 0 and m = ±2 channels—obviously higher than the backward scattering.

With the further increase of the collision energy to 2.07 eV, the DCS for m = ±2 channels resembled those at low collision energies as a broad peak but with the peak position moving forward further to θ = 60°. The DCS for the parallel configuration changed substantially and became rather uniform, with a broad peak at θ = 60° and another narrower peak in the forward direction, apparently as a result of a broader cone of acceptance and larger impact parameters. The direct combination of the m = 0 and m = ±2 DCSs without the interference terms looked close to m = ±2 with one peak in the forward direction and another at θ = 60° with the same heights. The interference between the m = 0 and m = ±2 channels substantially increased the peak intensity at θ = 60° and doubled the peak height, but it had no effect on the forward peak intensity, making the relative intensity of the forward-scattering peak considerably suppressed.

To verify this strong interference behavior, we show in Fig. 5, A and B, the comparison between experimental and theoretical DCSs for the product $H_2(v' = 0, j' = 1)$ and $H_2(v' = 1, j = 3)$ states, respectively, at the collision energy of 0.50 eV. As seen, the theory agreed with experiment well on the DCSs for both product states. The DCS for the $H_2(v' = 0, j' = 1)$ state exhibited two clear peaks at θ = 125° and 180°, respectively, whereas the direct combination without the interference terms only showed a tiny bump at θ = 120°. The DCS for the $H_2(v' = 1, j = 3)$ state exhibited two peaks with a pronounced one at θ = 90°; by contrast, the direct combination without the interference terms only had one broad peak. The interference effects were obvious for the perpendicular configuration.

The concept of intrinsic polarization-dependent differential cross sections (PDDCSs) has been widely used to study the stereodynamical effects in chemical reactions (*17*). Because the quantum dynamical simulation reproduces the observed DCSs very well, as shown in Fig. 3 (as well as the total DCSs, as shown in figs. S6 to S8), we can use the theoretical PDDCSs to analyze the observed stereodynamical effects. As shown in figs. S9 to S11,

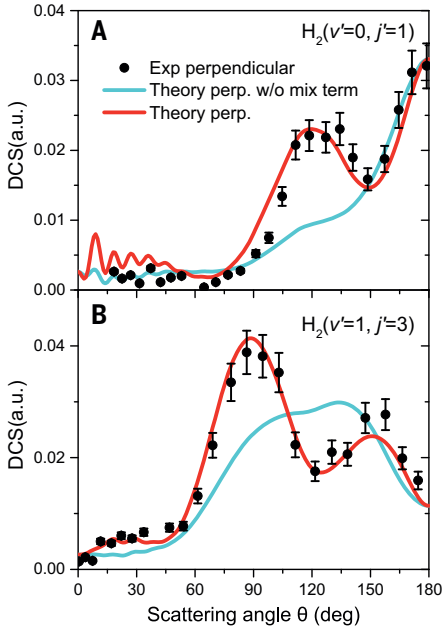

Fig. 5. Comparisons between experiment and theory on product state–resolved DCSs. (**A** and **B**) Comparisons are made on the scattering plane at the collision energy of 0.50 eV for the H_2 product in the (v' = 0, j' = 1) (A) and (v' = 1, j' = 3) (B) states. In this experiment, TOF spectra at different laboratory angles were acquired by scanning the laboratory angle back and forth 36 times. By analyzing the summed TOF signals for the above H_2 product states at each laboratory angle in these scans, the error bars of one standard deviation (1σ) in the experimental DCS shown in this figure were estimated to be ~10%. Analysis of experimental data and evaluation of error bars are also discussed in the supplementary materials.

the $S_0^{(2)}(\theta)$ and $S_0^{(4)}(\theta)$ moments are responsible for the effects in the parallel configuration as found in many theoretical studies (*12*, *17*, *19*), whereas the feature of stereodynamical effects in the sideways direction in the perpendicular configuration are mainly originated from the $S_{\pm2}^{(2)}(\theta)$ and $S_{\pm4}^{(4)}(\theta)$ moments.

Therefore, the m = 0 and m = ±2 channels for the HD(v = 1, j = 2) state had different angular distributions, with one backward dominated and the other peaked in a mostly sideways direction. For the perpendicular configuration, the angular distribution on the scattering plane is determined by Eq. 3, with the interference term between the m = 0 and m = ±2 channels. Notably, strong constructive interference occurred in the sideways direction, substantially enhancing the peak height in the sideways direction particularly at the collision energies of 1.20 and 2.07 eV. As a result, the measured angular distributions for the perpendicular configuration were markedly different from the parallel configuration, manifesting strong stereodynamical effects.

REFERENCES AND NOTES

1. R. N. Zare, *Science* **279**, 1875–1879 (1998).
2. F. F. Crim, *Acc. Chem. Res.* **32**, 877–884 (1999).
3. F. F. Crim, *Proc. Natl. Acad. Sci. U.S.A.* **105**, 12654–12661 (2008).
4. P. M. Hundt, B. Jiang, M. E. van Reijzen, H. Guo, R. D. Beck, *Science* **344**, 504–507 (2014).
5. B. R. Strazisar, C. Lin, H. F. Davis, *Science* **290**, 958–961 (2000).
6. H. Guo, B. Jiang, *Acc. Chem. Res.* **47**, 3679–3685 (2014).
7. G. Czakó, J. M. Bowman, *Science* **334**, 343–346 (2011).
8. K. Liu, *Annu. Rev. Phys. Chem.* **67**, 91–111 (2016).
9. B. L. Yoder, R. Bisson, R. D. Beck, *Science* **329**, 553–556 (2010).
10. R. B. Bernstein, D. R. Herschbach, R. D. Levine, *J. Phys. Chem.* **91**, 5365–5377 (1987).
11. D. H. Parker, R. B. Bernstein, *Annu. Rev. Phys. Chem.* **40**, 561–595 (1989).
12. F. J. Aoiz *et al.*, *Phys. Chem. Chem. Phys.* **17**, 30210–30228 (2015).
13. H. J. Loesch, *Annu. Rev. Phys. Chem.* **46**, 555–594 (1995).
14. Z. Karny, R. C. Estler, R. N. Zare, *J. Chem. Phys.* **69**, 5199–5201 (1978).
15. D. H. Parker, H. Jalink, S. Stolte, *J. Phys. Chem.* **91**, 5427–5437 (1987).
16. H. J. Loesch, A. Remscheid, *J. Chem. Phys.* **93**, 4779–4790 (1990).
17. J. Aldegunde *et al.*, *J. Phys. Chem. A* **109**, 6200–6217 (2005).
18. P. G. Jambrina, M. Morita, J. F. E. Croft, F. J. Aoiz, N. Balakrishnan, *J. Phys. Chem. Lett.* **13**, 4064–4072 (2022).
19. C. G. Heid, V. Walpole, M. Brouard, P. G. Jambrina, F. J. Aoiz, *Nat. Chem.* **11**, 662–668 (2019).
20. F. Wang, J. S. Lin, K. Liu, *Science* **331**, 900–903 (2011).
21. F. Wang, K. Liu, T. P. Rakitzis, *Nat. Chem.* **4**, 636–641 (2012).
22. H. Pan, F. Wang, G. Czakó, K. Liu, *Nat. Chem.* **9**, 1175–1180 (2017).
23. K. Liu, *J. Chem. Phys.* **142**, 080901 (2015).
24. G. C. Schatz, A. Kuppermann, *J. Chem. Phys.* **59**, 964–965 (1973).
25. J. Z. H. Zhang, S.-I. Chu, W. H. Miller, *J. Chem. Phys.* **88**, 6233–6239 (1988).
26. J. Jankunas *et al.*, *Proc. Natl. Acad. Sci. U.S.A.* **111**, 15–20 (2014).
27. Y. Xie *et al.*, *Science* **368**, 767–771 (2020).
28. T. Wang *et al.*, *Science* **342**, 1499–1502 (2013).
29. T. Yang *et al.*, *Science* **347**, 60–63 (2015).
30. T. Wang, T. Yang, C. Xiao, D. Dai, X. Yang, *J. Phys. Chem. Lett.* **4**, 368–371 (2013).
31. N. Mukherjee, R. N. Zare, *J. Chem. Phys.* **135**, 024201 (2011).
32. N. Mukherjee, W. Dong, R. N. Zare, *J. Chem. Phys.* **140**, 074201 (2014).
33. W. E. Perreault, N. Mukherjee, R. N. Zare, *Science* **358**, 356–359 (2017).
34. W. E. Perreault, N. Mukherjee, R. N. Zare, *Nat. Chem.* **10**, 561–567 (2018).
35. H. Zhou, W. E. Perreault, N. Mukherjee, R. N. Zare, *Science* **374**, 960–964 (2021).
36. X. Wang, X. Yang, *Science* **374**, 938–939 (2021).
37. M. Qiu *et al.*, *Rev. Sci. Instrum.* **76**, 083107 (2005).
38. Y. Wang *et al.*, *Rev. Sci. Instrum.* **91**, 053001 (2020).
39. D. Yuan *et al.*, *Science* **362**, 1289–1293 (2018).
40. Y. Wang *et al.*, Stereodynamical Control of the H+HD→H_2+D Reaction through HD Reagent Alignment, dataset, Dryad (2022); https://doi.org/10.5061/dryad.x0k6djhpk.

ACKNOWLEDGMENTS

We thank K. Liu for the helpful discussion on the stereodynamical experiment. **Funding:** This work was supported by the National Natural Science Foundation of China (grant nos. 22288201, 22173097, 41827801, and 22103084), the Chinese Academy of Sciences (grant no. GJJSTD20220001), the Innovation Program for

Quantum Science and Technology (grant no. 2021ZD0303300), the Guangdong Science and Technology Program (grant nos. 2019ZT08L455 and 2019JC01X091), and the Shenzhen Science and Technology Program (grant no. ZDSYS20200421111001787).
Author contributions: Y.W., W.W., T.D., Y.X., Y.M., C.X., and X.Y. performed the crossed-beam experiments and data analysis. J.H., Z.Z., and D.H.Z. performed the quantum dynamics calculations and data analysis. C.X., Z.Z., D.H.Z., and X.Y. designed the research and wrote the manuscript. **Competing interests:** The authors declare no competing interests. **Data and materials availability:** All data needed to evaluate the conclusions in this paper are present in the paper or the supplementary materials. All data presented in this paper are deposited at Dryad (*40*).

SUPPLEMENTARY MATERIALS

science.org/doi/10.1126/science.ade7471
Materials and Methods
Figs. S1 to S15
Table S1
References (*41*–*46*)

Submitted 12 September 2022; accepted 14 December 2022
10.1126/science.ade7471